SOOTING LIMITS OF DIFFUSION FLAMES WITH OXYGEN-ENRICHED AIR AND DILUTED FUEL

P.B. Sunderland[1], D.L. Urban[2], D.P. Stocker[2], B.H. Chao[3], and R.L. Axelbaum[4*]

[1]NCMR
[2]NASA Glenn Research Center
Cleveland OH

[3]Dept. of Mechanical Engr.
University of Hawaii
Honolulu HI

[4]Dept. of Mechanical Engr.
Washington University
St. Louis MO

INTRODUCTION

Oxygen-enhanced combustion permits certain benefits and flexibility that are not otherwise available in the design of practical combustors, as discussed by Baukal (1998). The cost of pure and enriched oxygen has declined to the point that oxygen-enhanced combustion is preferable to combustion in air for many applications. Carbon sequestration is greatly facilitated by oxygen enrichment because nitrogen can be eliminated from the product stream. For example, when natural gas (or natural gas diluted with CO_2) is burned in pure oxygen, the only significant products are water and CO_2. Oxygen-enhanced combustion also has important implications for soot formation, as explored in this work.

Most fundamental sooting limits have come from studies of laminar premixed flames. One reason for this is that both temperature and the C/O atom concentration ratio are nearly constant in the soot forming regions of premixed flames. The limits typically are identified by the C/O ratio at which luminous yellow emission is barely perceptible. The limits are intrinsic properties of the mixtures and offer both practical value and fundamental information about soot inception processes. When a limit occurs at a high C/O ratio for a given flame temperature this indicates conditions, e.g. fuel type, that are less conducive to forming soot. Takahashi and Glassman (1984) concluded that sooting limits in premixed flames arise from a competition between fuel pyrolysis and oxidative attack. Markatou et al. (1993) found that oxidation of light hydrocarbons (such as C_2H_3), rather than oxidation of polyaromatic hydrocarbons (PAH), is the mode of oxidation that is critical to sooting limits for premixed flames. The formation of PAH and soot is prevented by the oxidation of these light hydrocarbons.

Despite the differences between soot inception in premixed and nonpremixed flames, the C/O ratio (which varies with position in diffusion flames) is proposed here to be relevant to sooting limits in diffusion flames. Du and Axelbaum (1995) employed the C/O ratio to explain their observations of what later came to be called permanently-blue flames. The fundamental point here originates from the same reasoning as to why C/O ratio is relevant in premixed flames. When the C/O ratio is unity, there is exactly enough oxidizer to retain the carbon in the gas phase as CO, while at higher C/O ratio there is insufficient oxidation to gasify the carbon and this would be expected to lead to soot formation. Owing to finite-rate chemistry and the production of H_2O and CO_2 the measured sooting limit, $(C/O)_c$, in premixed ethylene/air combustion is less than unity. For ethylene it occurs around $(C/O)_c = 0.6$.

We propose that soot inception in nonpremixed flames requires a region where C/O ratio, temperature, and residence time are above certain critical values. Soot does not form at low temperatures, with the threshold in nonpremixed flames ranging from about 1250-1650 K, a

* Corresponding author.
Seventh International Combustion Workshop, Cleveland, 2003.

temperature referred to here as the critical temperature for soot inception, T_c. Soot inception also can be suppressed when residence time is short (equivalently, when the strain rate in counterflow flames is high). Soot induction times of 0.8-15 ms were reported by Tesner and Shurupov (1993) for acetylene/nitrogen mixtures at 1473 K.

The above reasoning is employed in Fig. 1 to explain the role of local C/O ratio and temperature, T, in unstrained nonpremixed flames. This figure depicts two diffusion flames, both with Z_{st} = 0.226 (where Z_{st} is the stoichiometric mixture fraction) and the same relationship between C/O and Z but with dramatically different adiabatic flame temperatures, T_{ad}, owing to different amounts of inert in the flames. For purposes of discussion, we assume here that T_c = 1250 K and $(C/O)_c = 1$. Consider first a flame of pure C_2H_4 and O_2 indicated by the dotted line. As indicated by the horizontal bar, a broad region exists where both $T > 1250$ K and C/O > 1; this region is expected to form soot given sufficient residence time. Consider next the other flame, shown in Fig. 1 by a dashed line, where both ethylene and oxygen have been diluted with nitrogen such that Z_{st} is unchanged but T_{ad} has been reduced until a condition is reached where C/O = 1 at the location where the local temperature is 1250 K. The conditions of the second flame characterize a flame at the sooting limit because the region where C/O ratio and temperature are both above their critical values is infinitely thin.

Burner stabilized spherical microgravity flames are employed in this work for two main reasons. First, this configuration offers unrestricted control over convection direction. Second, in steady state these flames are strain-free and thus can yield intrinsic sooting limits in diffusion flames, similar to the way past work in premixed flames has provided intrinsic values of C/O ratio associated with soot inception limits.

RESULTS AND DISCUSSION

The present experiments were conducted in microgravity in the NASA Glenn 2.2-second drop tower. The experimental apparatus is described in detail in Sunderland et al. (2003). As before, the burner is a 6.4 mm diameter porous stainless-steel sphere. All tests were conducted in quiescent ambient gas at 295 K and 0.98 bar (with an estimated uncertainty of ±0.005 bar), and ignition was performed in microgravity.

Four representative flames at or near their sooting limits are shown in Fig. 2. Typical of the flames in this study, these images reveal spherical symmetry except near the burner tube. These flames represent both convection toward oxidizer (normal flames) and convection toward fuel (inverse flames). The flames of Fig. 2b and 2d are considered here to be at the experimental sooting limits since a small reduction in reactant concentration yields blue conditions. Note that soot, when present, appears inside the flame sheet for normal flames and outside for inverse flames.

Seventeen sooting limits have been identified. The sooting limits of are presented in Fig. 3 in terms of reactant compositions. The present spherical flames allow a boundary to be identified between conditions where soot cannot form in unstrained, long residence time flames – permanently-blue flames – and conditions where soot can form given sufficient residence time. This boundary is identified by the solid curve. The dashed curves are T_{ad} isotherms, determined with CEA. Within experimental uncertainties convection direction does not have an impact on the sooting limits. Figure 3 also includes sooting limits measured in normal-gravity counterflow C_2H_4 flames in three previous studies, namely Du and Axelbaum (1995), Lin and Faeth (1996), and Hwang and Chung (2001).

Further insight can be gained by plotting the present sooting limit data in terms of T_{ad} versus Z_{st}. Recall that Fig. 1 used $(C/O)_c$ and T_c to identify where soot can and cannot form in unstrained nonpremixed flames. In other words, if $(C/O)_c$ occurs at the same location as T_c on the fuel side, conditions suitable for soot formation are infinitely thin, indicating a sooting limit given sufficient residence time. Employing the Burke-Schumann assumptions, Y_C, Y_O and T are linear in Z, as in Fig. 1. This behavior, coupled with the hypothesis that soot formation requires temperature and C/O to be above fixed critical values, predicts a linear increase in T_{ad} with Z_{st} at the sooting limit. Motivated by this analysis, the data in Fig. 3 are plotted in Fig. 4 in terms of Z_{st} versus T_{ad}, again defining a region of permanently-blue conditions. Figure 4 allows the data to be correlated with a least-squares fit, yielding the fit shown. This correlation also is included as the solid curve in Fig. 3, where the mapping from the axes of Fig. 4 to those of Fig. 3 was done using CEA. The slope of the line fit in Fig. 4 reveals the large effect of Z_{st} on sooting limits, accounting for a range in T_{ad} at the sooting limits of 1815 to 2738 K. Figure 4 shows that convection direction has no measurable effect on the sooting limits of the present flames. The normal-gravity sooting limit flames in Fig. 3 also are included in Fig. 4.

Figure 4 indicates that the mechanism for attaining a sooting limit may be different at low and high Z_{st}. The adiabatic flame temperature for the low Z_{st} sooting-limit flame is nearly equal to T_c. Thus, when inert is added to the standard fuel/air flame (low Z_{st}) the sooting limit is obtained largely because the temperature is so low that the kinetics of soot inception are too slow to produce soot. On the other hand, when Z_{st} is high, C/O ratio is high deep into the fuel side of the flame. This suggests the sooting limit is attained because there is sufficient oxygen on the fuel side of the flame to favor oxidation of light hydrocarbons over formation of soot precursors. C/O ratio is higher farther into the fuel-rich region but there the temperature is too low for soot inception to occur.

Acknowledgments: This research was funded by the National Aeronautics and Space Administration under grants NCC3-697 and NAG3-1910 (RLA), and NCC3-696 and NAG3-1912 (BHC) under the technical management of M.K. King. Assistance with the microgravity tests was provided by C.A. Johnston and B.J. Goldstein. Programmatic support was provided by R.C. Forsgren.

REFERENCES

Baukal, C.E., Oxygen-enhanced combustion, C.E. Baukal, Ed., CRC Press, Boca Raton, pp. 1-45 (1998).

Du, J. and Axelbaum, R.L., Combust. Flame 100:367 (1995).

Hwang, J.Y. and Chung, S.H., Combust. Flame 125:752 (2001).

Lin, K.–C. and Faeth, G.M., J. Propulsion and Power 12:691 (1996).

Markatou, P. Wang, H. and Frenklach, M., Combust. Flame 93:467 (1993).

Sunderland, P.B., Axelbaum, R.L., Urban, D.L., Chao, B.H. and Liu, S., Combust. Flame 132:25 (2003).

Takahashi, F. and Glassman, I., Combust. Sci. Tech. 37:1 (1984).

Tesner, P.A. and Shurupov, S.V., Combust. Sci. Tech. 92:71 (1993).

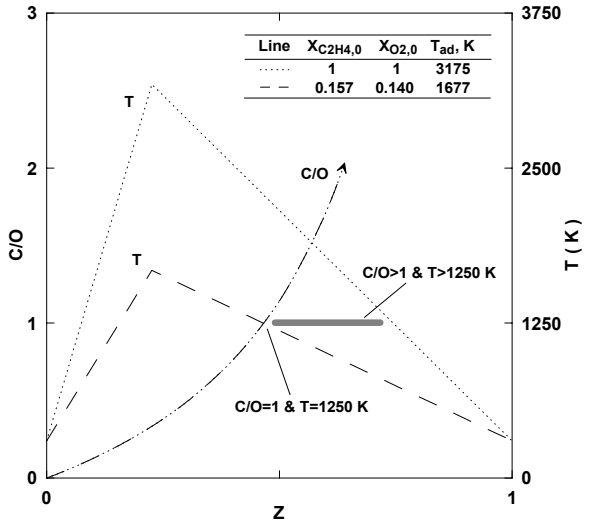

Fig. 1. Profiles in mixture-fraction space of T_{ad} and C/O ratio for two flames with Z_{st} = 0.226 but different flame temperatures. The Burke Schumann assumptions have been made. The horizontal bar indicates the region of potential soot inception for the high temperature flame. Such a region does not exist for the low temperature flame.

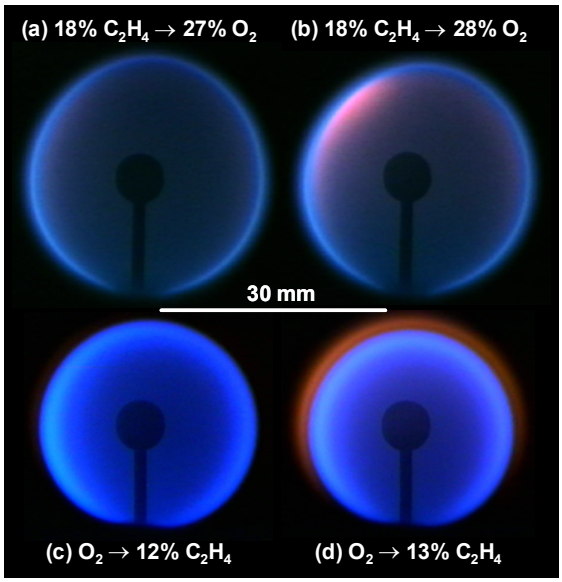

Fig. 2. Color images of representative flames below the sooting limit (a and c) and at the sooting limit (b and d) for convection toward oxidizer (a and b) and convection toward fuel (c and d). Images were taken just before drop termination.

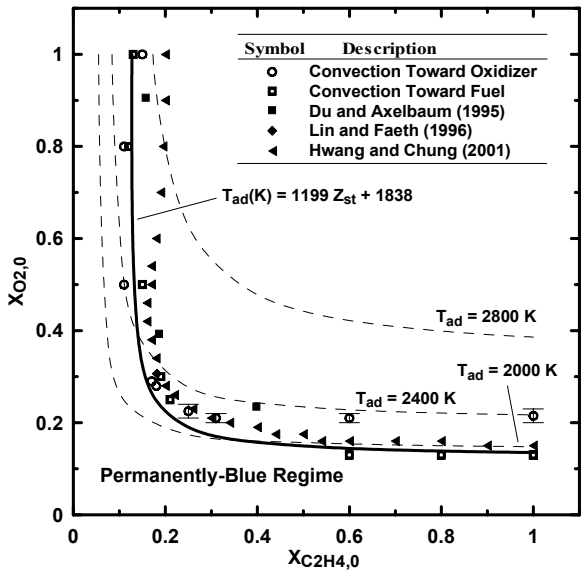

Fig. 3. Oxygen mole fraction versus ethylene mole fraction in the supply gases at the sooting limit for the present flames and for published normal-gravity flames.

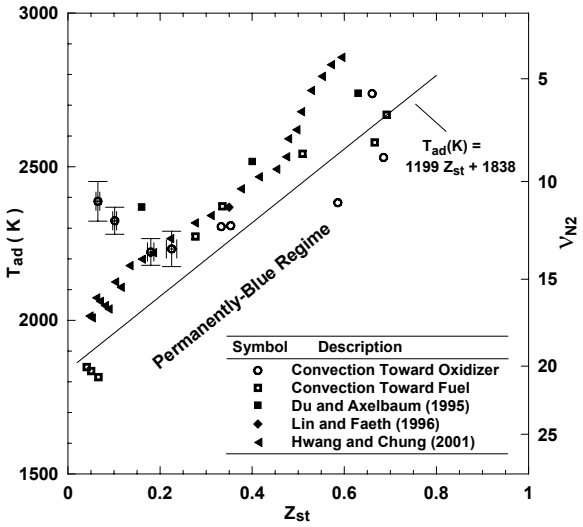

Fig. 4. Adiabatic flame temperature versus stoichiometric mixture fraction at the sooting limit for the present flames and for published normal gravity flames. The ordinate symbol ν_{N2} is associated with the stoichiometry of $C_2H_4 + 3O_2 + \nu_{N2}N2 \rightarrow$ products, and corresponds to the T_{ad} shown.